Spray Characteristics and Droplet Size Distributions From Low Pressure Spray Atomisation

K.Inthavong[1], W.Yang[2], M.C.Fung[1], X.W.Tong[1] and J.Y.Tu[1]

[1]School of Aerospace Mechanical Manufacturing Engineering

RMIT University, East Bundoora Campus, 3083, Australia

[2]CSIRO Process Science and Engineering,
Clayton South, Victoria, Australia

Abstract

An understanding of the physical mechanisms underlying the atomization process from a spray device can reveal important information leading to more effective device design. A commercial nasal spray device exhibiting low pressure atomization was tested to obtain spray formation, its characteristics, droplet size distribution, and droplet velocity. High speed laser photography combined with an in house designed automated actuation system, and a highly precise traversing unit, measurements and images magnified in small field of view regions within the spray was performed. The spray formation was produced from a swirling liquid sheet that separated off into ligaments, and continued to breakup into droplets. These droplets continued to deform as they travel downstream at velocities of up to 20 m/s.

Introduction

Atomization of a liquid causes an increase of surface area which is of significance for onset of action via chemical reactions in transferring the therapeutic benefits for drug penetration through the respiratory mucus walls upon its deposition. Therefore understanding of spray atomization can lead to more effective drug delivery means.

Spray atomization studies have traditionally focussed on high pressure applications e.g. approximately 100Bar found in engine combustion [1] which has left of data related to low pressure applications lagging behind. More recently however, there has been increased interest in low pressure applications. This includes oral and nasal spray drug delivery, where a better understanding of the fluid dynamics and atomisation of the liquid drug formulation into fine droplets can lead to targeted drug delivery for greater efficiency[2]. For example past studies revealed that larger droplets and a wider spray angle were inefficient because the droplets mainly deposited in the front nasal area and failed to reach the middle nasal cavity [3-6].

Several experimental studies for determining such spray characteristics have been performed which provide good contribution toward a set of data. These results include Dayal et al. [7] studied the impact of actuation mechanisms and drug formulation properties on the droplet size distribution to conclude that they all played a role in determining the droplet size distribution. In a later study, Guo and Doub [8] performed a similar study that related to the spray characteristics to actuation velocity and acceleration instead of actuation force.

In terms of the droplet size distribution, Cheng et al. [3] found single-mode and bimodal droplet size distribution (DSD) variations between four spray pumps and provided a lognormal distribution profile of the DSD. The $Dv10$, $Dv50$, and $Dv90$ values have been measured by Fung et al. [9, 10], Suman et al. [4], Dayal et al. [7], Foo et al. [11], and Guo et al. [8] for three different spray pumps and different drug formulations. In these studies, laser diffraction has been used to characterize the DSDs by the cumulative volume mean diameters (VMDs) at $Dv10$, $Dv50$, and $Dv90$, respectively. The laser diffraction technique is based on the scattering of light from a collimated laser beam as it hits the droplet that passes through it. The scattered light then hits a detector at different angles, inversely proportional to the particle's size; thus, the droplets of the same size will scatter light to the same part of the detector array. As a result, there is a scattering pattern on the detector and a DSD can be determined by fitting the data with a scattering algorithm/model typically supplied with the laser imaging system.

The accuracy of the DSD therefore has a reliance on the scattering model. One other issue in relation to laser diffraction is the selection of the spray tip to laser distance. Since the spray formation can develop over 50 cm in length [4], the DSD will vary significantly if the laser beam is passed across the spray close to the spray nozzle compared with a distance far from the nozzle distance.

Computational fluid dynamics (CFD) simulations have been performed to model the transport and deposition of particles in realistic nasal cavities during inhalation [12-17]. Typically, the particles are introduced into the flow domain after a steady state simulation has been performed and hence a one-way gas-particle coupling approach is used.

This paper presents experimental work to measure spray parameters including spray cone angle, initial particle velocity, insertion angle, particle size, and particle release location. This will lead to improvements to the current state of CFD simulations where realistic initial droplet conditions produced during spray atomization can be applied.

Method

An in-house automated actuation system was developed, which uses a pneumatic actuator with a two-way solenoid valve controlled by a programmable logic control unit. The spray bottle is a commercially available over-the-counter nasal spray device kindly provided by GlaxoSmithKline, capable of delivering 200

sprays per bottle with 50 μg of formulation per actuation during normal operation. A large water tank (20 L) filled with distilled water was attached to the nasal spray bottle to ensure a consistent water level in the nasal spray bottle and constant internal pressure. The spray bottle was fixed at the base on the actuator to avoid undesired lateral motion during actuation.

The automated actuation system comprised of a spray bottle holder, a programmable logic control unit (PLC), pneumatic valves and a pneumatic actuator. The spray bottle was fixed on a stand, thus the undesired lateral motion was avoided during actuation. The pressing and releasing motion on nasal spray bottle was executed by a pneumatic actuator. The actuation speed of pressing and releasing was managed by two speed controllers on the pressure line. The PLC unit was used to control the open and close motion of the pneumatic valves, and thus the motion of the actuator. The internal timers and counters of the PLC manipulate the time between actuations and the number of actuations. The strength of actuation force was produced by a back pressure of 2.05Bar. The nasal spray bottle was held in its initial position for 2.5 seconds before the next actuation. A time of 2.5 seconds between each actuation was determined by Particle and Droplet Image Analysis (PDIA) for sufficient settling of suspended spray droplets from the previous injection.

The high speed photography used a Particle/Droplet Image Analyser (PDIA) system that included a New Wave 120 mJ double-pulsed Nd:YAG laser with a SensiCam 12-bit digital charge-coupled device (CCD) camera (1,280×1,024 pixels). The spray images were captured with long distance micro-scope lens with magnification of 2.23 to achieve a physical size field-of-view (FOV) of 3.85 mm×3.08 mm with resolution of 3.01 μm/pixel. This means that to capture the near nozzle spray atomisation, six FOV regions are required. Figure 1 shows the FOVs where each row (R) is labelled, from R1 (closest to the spray orifice) to R3.
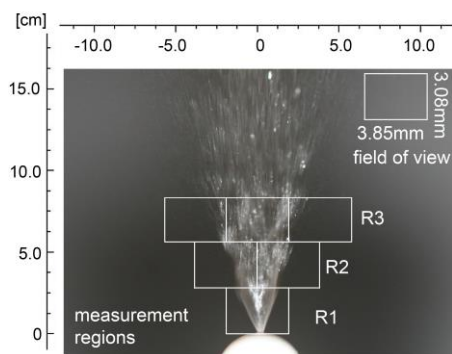

Figure 1. Field of View (FOV) regions used for analysis of the spray in the near nozzle region.

Results and Discussion

Spray Atomization Development

The actuation of the spray device took 229 ms. There is a delay between the beginning of actuation and the instance at which the liquid first discharges from the nozzle exit, because of the force required to overcome the internal atomizer. The total liquid spray discharge time was 144 ms.

Spray atomization development can be categorized into three stages (Inthavong et al. 2012; Fung et al. 2013) as the pre-, fully-, and post- developed stages. Within each stage the liquid sheet exhibits a unique pattern as it ejects from the nozzle (Figure 2). In the pre-developed stage a thin liquid sheet swirls out of the

nozzle in a tubular shape. The swirling nature is visualized in the ripples along the surface of the liquid sheet. In the fully developed stage, the spray has reached its full spray plume and its radial dispersion is complete producing its full spray cone. In this developed stage, the swirling effect produces large shearing forces on the surface of the liquid sheet. In the post-developed stage the atomized energy begins to dissipate and the insufficient force. The spray plume begins to collapse on itself and the shape returns to a tubular shape before dying out.

pre developed

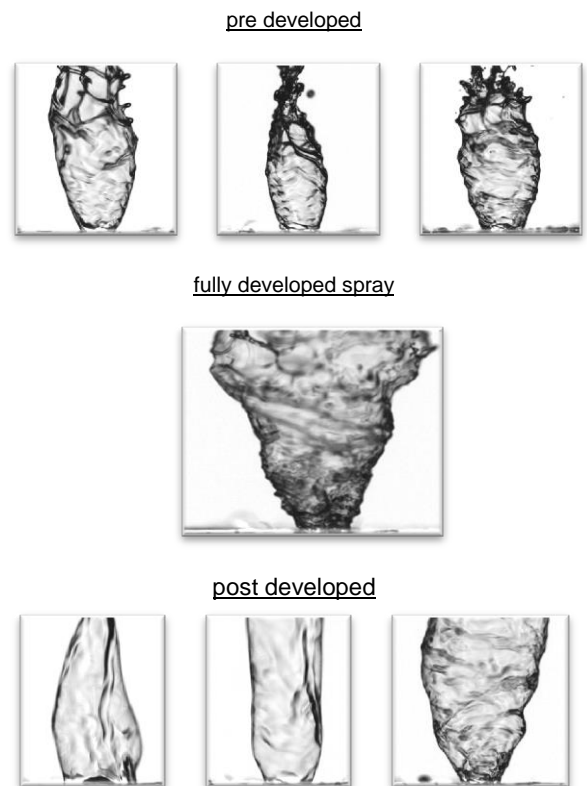fully developed spray

post developed

Figure 2. Near nozzle liquid sheet formation as the during spray atomization. The field of view is from 0mm-3.08mm from the nozzle exit.

Unstable wavelengths are found on the surface of the sheet due to the inherent swirl imparted onto the liquid by the internal pressure swirl atomizer. A theoretical model proposed by Dombrowski and Johns [18] describes the atomization process occurring due to the growth rate of surface waves that are dependent on surface tension, aerodynamic forces, and liquid viscosity. When these waves become sufficiently unstable liquid ligaments break off and then final droplets break off the ligaments (Figure 3).
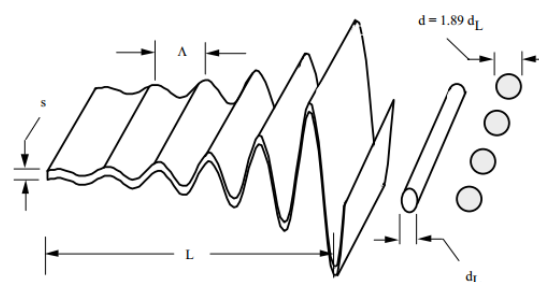

Figure 3 Schematic of the sheet disintegration and drop formation processes as proposed by Dombrowski and Johns (1978)

An additional theoretical model presented by Stapper et al. [19] describes the atomization by a `stretched stream-wise ligament breakup' regime where stream-wise vortical waves become amplified and thin liquid membranes are formed in between them. Eventually the membranes burst, forming small drops, while the vortical waves produce stream-wise ligaments which breakup into relatively large drops.

In the next row of images (3.08mm-6.16mm from the spray nozzle shown in Figure 4) the surface waves propagate and grow downstream. As a result the liquid sheet becomes thinner and surface wave instabilities in the form of sinusoidal oscillations increases and, the sheet begins to break up; first into small ligaments and then atomize to small droplets. It is in this set of images that the spray breakup length occurs, which is the distance between nozzle outlet and spray droplet formation.
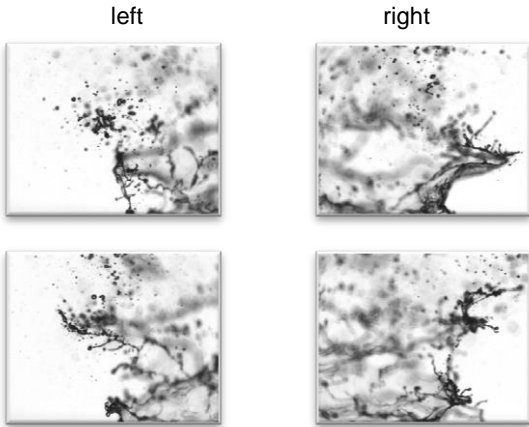
left   right

Figure 4. Instantaneous spray breakup images in the field of view (FOV) region 3.08mm to 6.16mm downstream from the nozzle. taken at two different time instances. In this region the spray break-up length occurs.

Further downstream at a distance of 6.16mm to 9.24mm the spray plume has dispersed radially now expanding three FOV regions, and hence the total width of the combined left, centre, and right FOVs in Figure 5 is equal to 11.55mm. In this region the liquid sheet has completely broken down and nearly all the liquid ligaments have also atomized into droplets. Established droplets are not necessarily spherical given the continual deformation as the droplets move through the quiescent surrounding air. The continual droplet deformation can lead to secondary breakup where the droplets breakup into subsequent smaller droplets (25-Lefebvre).
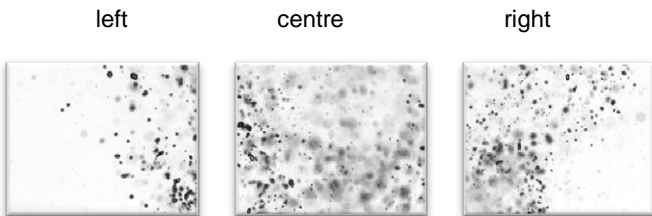
left   centre   right

Figure 5. Droplet formation from breakdown of the liquid sheet for the field of view region at a distance of 6.16mm to 9.24mm downstream from the nozzle exit.

Droplet Size Distribution

Droplet size distribution measurements, by volume mean diameter, are taken at actuation time, t_1=126ms. The measured droplet size distribution is obtained from the row R3, where droplet formation is taking place. The droplet size distribution is a skewed distribution with a peak ranging between 50 μm and 110 μm.

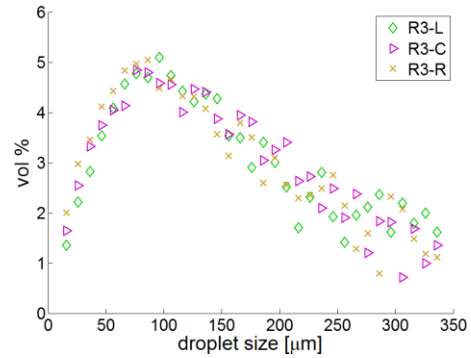Figure 6. Droplet size distribution taken at an instantaneous time t_1=126ms along row R3.

Droplet Velocity

Droplet velocities were obtained from two sequential snapshots separated by 6 μs in time using the PDIA visualization system. A sample image pair with grid spacing of 337 μm shows the droplets' trajectory and its velocity determined through the distance of its trajectory over the period of time (Figure 7). The image contains droplets deforming and rotating as it moves further downstream. This suggests the droplet size is dynamic and has potential to further atomize during its secondary breakup.
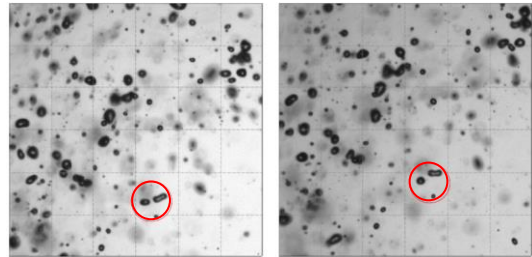

Figure 7. Spray images in sub-regions within the FOV region of row R3. Each image is separated by 6 μs in time. The initial image is brighter than the latter as the influence of the flash diminishes over the short period of time. Each square grid is 337 μm microns in size. The highlighted circle is an example of tracking individual droplets and its trajectory between the paired images

The average droplet velocity across the spray width for the left, centre, and right FOV regions along row R3 are shown in Figure 8. The velocities were measured for two time instances t_1 = 126ms and t_2= 168ms. Peak velocities reach up to 20m/s while the low velocities were approximately 10m/s.
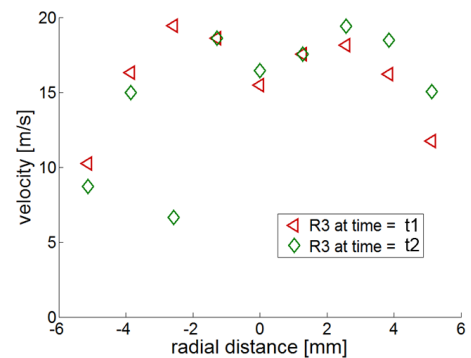
Figure 8. Averaged droplet velocity across the row R3 taken at actuation time t_1=126 ms and t_2=168ms.